Hyperfine Interact
DOI 10.1007/s10751-013-0919-1

Mössbauer and XRD study of pulse plated Sn-Fe, Sn-Ni and Sn-Ni-Fe electrodeposited alloys

S. Stichleutner · G. B. Lak · E. Kuzmann · C. U. Chisholm · M. El-Sharif · Z. Homonnay · L. Sziráki

Abstract Effect of pulse plating on novel electrodeposited binary and ternary amorphous alloys was studied by ^{57}Fe and ^{119}Sn conversion electron Mössbauer spectroscopy and X-ray diffraction. Our results show that by adjusting the parameters of pulse plating a fine tuning of the composition and current efficiency can be achieved within these systems. On the contrary to direct current deposition, where the crystalline $FeSn_2$ phase dominates, pulse plating technique produces amorphous Sn-Fe alloy phases, of which the ferromagnetic phase is the dominant one. Both, direct current and pulse plated Sn-Ni deposits consist of paramagnetic alloy phases and minor amounts of β-Sn, the occurrence of which correlates with the tin content of the samples. Pulse plated Sn-Ni-Fe coatings are amorphous and in a dominantly ferromagnetic state, however at long on- and off-pulse times and high peak current density the paramagnetic state dominates and β-Sn segregation also occurs.

Keywords Sn-Fe and Sn-Ni binary alloys · Sn-Ni-Fe ternary alloys · Electrodeposition · Amorphous alloys · ^{57}Fe and ^{119}Sn Mössbauer spectroscopy

Proceedings of the 32nd International Conference on the Applications of the Mössbauer Effect (ICAME 2013) held in Opatija, Croatia, 1–6 September 2013.

S. Stichleutner
Centre for Energy Research, Hungarian Academy of Sciences, Budapest, Hungary

S. Stichleutner · E. Kuzmann (✉) · Z. Homonnay · L. Sziráki
Institute of Chemistry, Eötvös Loránd University, Budapest, Hungary
e-mail: kuzmann@ludens.elte.hu

G. B. Lak · C. U. Chisholm · M. El-Sharif
Glasgow Caledonian University, Glasgow, Scotland, UK

Published online: 25 October 2013

1 Introduction

Novel electrodeposited tin-based alloys such as Sn-Co-Fe, Sn-Ni-Fe, and Sn-Fe, which can give nano level structures, are considered as future electrode materials for Li-ion battery applications [1, 2]. In our previous works, we succeeded in establishing direct current (DC) plating conditions to deposit good quality binary (Sn-Fe [3–5]) and ternary (Sn-Co-Fe [3, 4, 6], Sn-Ni-Fe [7, 8]) alloys in a wide composition range. Extensive Mössbauer spectroscopy and X-ray diffraction (XRD) studies performed on these alloys showed that samples deposited at low current density mainly exhibit crystalline phases of known compounds while in those deposited at high current density new amorphous phases are the dominant ones. The analysis of a large number of spectra of binary and ternary alloys electrodeposited under variable plating conditions suggested a model for the short-range order of the new amorphous alloy phases where the atoms in the highly disordered structures would be randomly distributed [1].

Pulse electrodeposition technique can utilize high peak current density, has the advantage of having a more even distribution of the ions in the bath due to the migration during the off-pulse time and has been known to produce finer grained deposits with better properties than conventionally plated coatings [9]. The purpose of the present work was to study the influence of the preparation parameters on composition, short-range order and on the phases formed in novel Sn-Fe, Sn-Ni and Sn-Ni-Fe pulse plated alloys.

2 Experimental

Batches of Sn-Fe, Sn-Ni and Sn-Ni-Fe samples were pulse plated under varying deposition conditions (Table 1) in a glass cylindrical cell with agitation at 20°C. The pulse plating signal used was square-wave and the parameters of the deposition presented in Table 1 are illustrated on Fig. 1. t_{on} reflects the on-pulse time, when the deposition takes place. t_{off} represents the relaxation time when the solution around the cathode can be refreshed. I_p denotes the applied peak current density, while I_m represents the mean or average current density during the deposition and γ is the duty ratio between the on-pulse time and the period of one pulse. To provide a direct comparison, DC deposited samples were also prepared in the case of Sn-Fe and Sn-Ni (Table 2). The composition of the electrolyte used for each deposition is listed in Table 3. The anode used was of high density carbon and was placed in 1.5 cm distance from the cathode on either side. The samples were deposited onto a 250 μm thick copper foil, which was treated in 66 wt% phosphoric acid solution at a constant current density of 0.5 A cm^{-2} for 2 min and thereafter rinsed in demineralised water prior to pulse plating.

Composition of the deposits was determined by Energy Dispersive Spectroscopy using a Peltier-cooled single crystal silicon detector made by Oxford Instruments Ltd., and the spectra were evaluated by the internal built-in XPP calibration of the AZTEC software. X-ray diffractograms of the electrodeposited samples were recorded using a computer controlled powder diffractometer (DRON-2).

^{57}Fe and ^{119}Sn conversion electron Mössbauer (CEM) spectra were recorded by a conventional Mössbauer spectrometer (WISSEL) with a flowing gas (96 % He,

Table 1 Deposition parameters and composition of pulse plated Sn-Fe, Sn-Ni and Sn-Ni-Fe samples

Sample code	Deposition							Sample composition				
	Peak current density (mA/cm^2)	t_{on} (s)	t_{off} (s)	Duty ratio (%)	Average current density (mA/cm^2)	Time (s)	Mass (mg)	Sn Wt%	Ni Wt%	Fe Wt%	Thickness (μm)	Current efficiency (%)
SnFe I	62.5	0.01	0.49	2.00	1.3	150	0.1	93.74	0.00	6.26	0.08	58
SnFe IV	333.3	0.01	0.49	2.00	6.7	150	0.4	71.35	0.00	28.65	0.44	72
SnFe VIII	83.3	0.01	0.09	10.00	8.3	150	0.3	72.87	0.00	27.13	0.33	42
SnFe X	71.4	0.03	0.47	6.00	4.3	150	0.4	68.09	0.00	31.91	0.38	98
SnNi I	62.5	0.01	0.49	2.00	1.3	150	0.1	90.40	9.60	0.00	0.08	60
SnNi III	200.0	0.01	0.49	2.00	4.0	150	0.3	88.34	11.66	0.00	0.27	61
SnNi VIII	85.5	0.01	0.09	10.00	8.6	150	0.3	92.50	7.50	0.00	0.34	35
SnNi X	76.9	0.03	0.47	6.00	4.6	150	0.3	87.40	12.60	0.00	0.31	61
SnNiFe I	100.00	0.01	0.49	2.00	2.0	300	0.5	71.72	1.67	26.61	0.33	89
SnNiFe VI	83.3	0.01	0.09	10.00	8.3	300	0.5	69.56	2.19	28.25	0.55	36
SnNiFe X	71.4	0.05	0.45	10.00	7.1	300	0.6	67.24	0.53	32.23	0.57	44
SnNiFe XIV	279.7	0.1	0.9	10.00	28.0	300	0.5	79.48	3.37	17.16	0.47	8

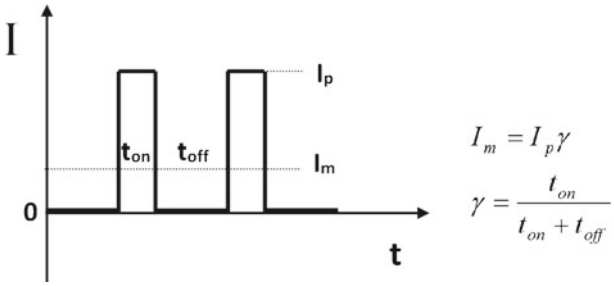

Fig. 1 Schematic representation of the square-wave pulse and the parameters of the deposition (see explanation in text)

4 % CH_4) proportional counter (RANGER) at room temperature. Isomer shifts are given relative to α-Fe. The evaluation of Mössbauer spectra was performed by least-square fitting of the lines using the MOSSWINN program [10].

3 Results and discussion

3.1 Effect of pulse plating parameters on alloy composition and current efficiency

It can be seen from Table 1, that pulse plating parameters have significant effect on the composition and current efficiency. Smaller current efficiency refers to higher amount of hydrogen evolution or other reducible species in the bath. Hence the thickness of the deposit is determined by the average current density and current efficiency.

In case of the Sn-Fe and Sn-Ni binary baths (Table 3), pulse plating parameters were set in order to investigate the effect of the 3–6 fold increase of peak current density at constant duty ratio (samples SnFe I, SnFe IV, SnNi I, SnNi III). Furthermore, for all, the binary and ternary Sn-Ni-Fe baths, we investigated the decrease of relaxation time at constant pulse current density and on-pulse time (samples SnFe I, SnFe VIII, SnNi I, SnNi VIII, SnNiFe I, SnNiFe VI). Finally, the effect of increasing the on-pulse time was investigated at constant pulse current density and relaxation time (samples SnFe I, SnFe X, SnNi I, SnNi X, SnNiFe I, SnNiFe X). Changing these parameters leads to a 3–5 fold increase in the duty ratio parameter.

Comparing samples SnFe I and SnFe IV, the dramatic changes in the pulse current density cause a significant drop in tin content, hence the deposition thickness and current efficiency increases. Comparing sample SnFe I with SnFe VIII, the decrease of relaxation time causes similar effect on composition as the increase of the current density during the pulse. Tin content drops significantly, however, a slight decrease of current efficiency can be observed. Comparing sample SnFe I to SnFe X, the small increase of the on-time pulse and duty ratio induces further increase of iron content and results in the lowest tin content in the regime. Current efficiency is 98 %, which is an outstanding result.

Comparing sample SnNi I with SnNi III, the increase of pulse current density causes only a slight drop in tin content, hence the deposition thickness increases and current efficiency stays about the same. Comparing sample SnNi I to SnNi VIII, the decrease of relaxation time causes opposite effect on composition to the increase of current density during the pulse. Tin content increases slightly, however, a major

Table 2 Deposition parameters and composition of direct current plated Sn-Fe and Sn-Ni samples

Sample code	Deposition							Thickness (μm)	Current efficiency %
	Potential (V)	Average current density (mA/cm^2)	Time (s)	Mass (mg)	Sn Wt%	Ni Wt%	Fe Wt%		
SnFe P8	−1.6	8.5	100	1.0	72.57	0.00	27.43	0.39	73 %
SnNi P7	−1.5	5.6	100	0.2	88.91	11.09	0.00	0.20	49 %

Table 3 Electrolyte composition used in the deposition of Sn-Fe, Sn-Ni and Sn-Ni-Fe samples

Compounds	Concentration of the compounds (M)		
	Sn-Fe	Sn-Ni	Sn-Ni-Fe
NaCl	0.3	0.3	0.3
H_3BO_3	0.3	0.3	0.45
Na-gluconate	0.4	0.4	0.5
Ascorbic acid	2 g/l	2 g/l	2 g/l
$SnSO_4$	0.066	0.057	0.04
$NiSO_4$	–	0.143	0.085
$FeSO_4$	0.134	–	0.075
Peptone	0.1 g/l	0.1 g/l	0.1 g/l
pH	6.00	6.00	6.00

decrease in current efficiency is observed. Comparing samples SnNi I and SnNi X, the small increase of the on-pulse time and duty ratio induces a small increase of nickel content and results in the lowest tin content in the regime. The observed current efficiency stays the same as for SnNi I.

In case of the ternary bath, comparing sample SnNiFe I to SnNiFe VI, the decrease of relaxation time causes a small drop in tin content and increases both the nickel and iron content within the deposit. The deposition thickness increases, however, current efficiency decreases. Comparing samples SnNiFe I and SnNiFe X, the small increase of the on-pulse time and duty ratio induces further increase of iron content and results in the lowest tin content in the regime. Nickel content decreases to the detection limit. Current efficiency is 44 %, which value is similar to the relaxation time effect results. Comparing sample SnNiFe I with SnNiFe XIV, the huge increase of the pulse current density with tenfold increase of the on-pulse time and twofold increase of the off-pulse time induces increase of tin and nickel content and results in the lowest iron content in the regime. Current efficiency is 8 %, which is the lowest result.

3.2 Characterization of the samples by Mössbauer spectroscopy and XRD

The ^{57}Fe spectrum of the DC deposited Sn-Fe sample (Fig. 2a) was decomposed into a magnetically split sextet with broad lines and a singlet. The sextet is characteristic of amorphous alloys and is considered as a superposition of a number of subspectra belonging to iron atoms being in slightly different microenvironments. The sextet was attributed to a ferromagnetic amorphous Sn-Fe phase, while the singlet was identified with the crystalline $FeSn_2$ phase. The larger line width of the singlet suggests a microcrystalline nature of the $FeSn_2$ phase. In accordance, the ^{119}Sn spectrum of the DC deposited Sn-Fe sample (Fig. 2b) was decomposed into a broad magnetically split sextet, assigned to the ferromagnetic amorphous Sn-Fe phase, and a doublet, representing the crystalline $FeSn_2$ phase. In both spectra, the crystalline $FeSn_2$ phase is the dominant one. This was also supported by the x-ray diffractogram of the DC deposited Sn-Fe sample, where peaks belonging to the $FeSn_2$ phase appeared, while in the case of the pulse plated samples only amorphous peaks were present. Pulse plating at the lowest peak current density (sample SnFe I) produces a rather thin Sn-Fe deposit with the lowest content of iron making the evaluation of the ^{57}Fe spectrum (Fig. 2c) inconclusive. Because of the high tin content, the ^{119}Sn spectrum (Fig. 2d) of this sample could be well evaluated and was decomposed into

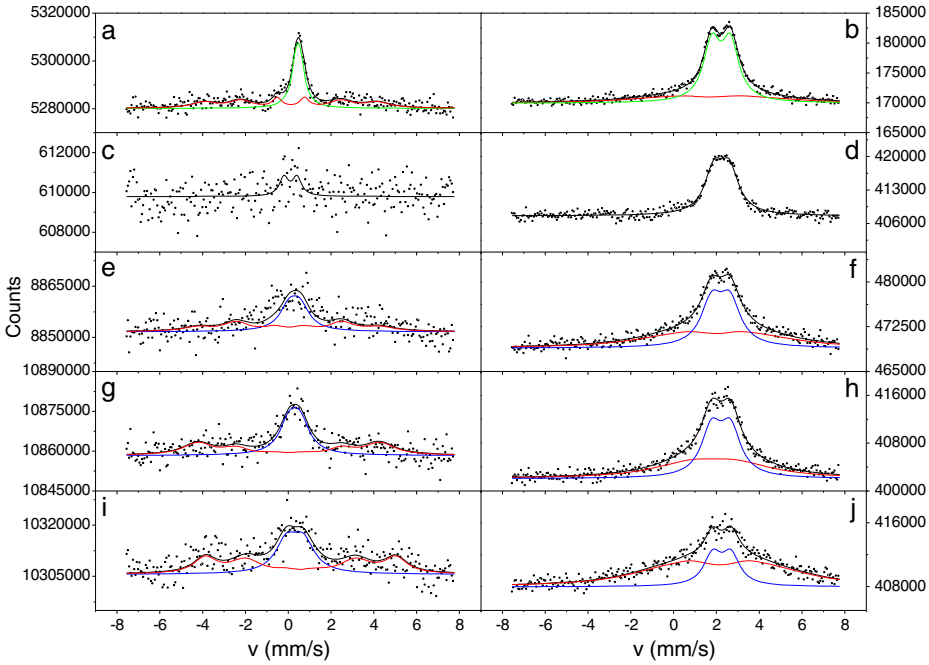

Fig. 2 ^{57}Fe (*left*) and ^{119}Sn (*right*) Mössbauer spectra of pulse plated Sn-Fe deposits

a dominant doublet with broad lines and a sextet with similarly broad lines with a rather small (3 %) relative amount. The doublet was assigned to a paramagnetic amorphous Sn-Fe phase, while the sextet to a ferromagnetic one. Using the same on-/off-pulse time and applying a higher peak current density (sample SnFe IV) results in a thicker, iron rich deposit. Both, the ^{57}Fe and ^{119}Sn spectra (Fig. 2e and f) of sample SnFe IV were decomposed into a magnetically split sextet and a doublet with broad lines, which were assigned to a ferromagnetic amorphous and a paramagnetic amorphous Sn-Fe phase, respectively. Decreasing the relaxation time and peak current density (sample SnFe VIII) creates ion depleted areas around the cathode producing a deposit with lower iron content as compared to sample SnFe IV deposited at a higher peak current density. The ^{57}Fe and ^{119}Sn Mössbauer spectra (Fig. 2g and h) of sample SnFe VIII are similar to those of sample SnFe IV and were evaluated accordingly, which, alongside the wide doublets, resulted in sextets with smaller hyperfine fields due to lower iron content. In the spectra of both, sample SnFe IV and SnFe VIII the ferromagnetic amorphous Sn-Fe phase is the dominant one by a slight margin. Increasing the on-pulse time (sample SnFe X) results a deposit with the highest iron content. The evaluation of the Mössbauer spectra (Fig. 2i and j) of sample SnFe X was performed similarly to the previous pulse plated samples and resulted in sextets with higher hyperfine fields. The ferromagnetic amorphous phase exhibited a further increase in its spectral amount on the expense of the paramagnetic one. In comparison to the DC deposited sample, no crystalline $FeSn_2$ phases could be identified in the Mössbauer spectra of the pulse plated deposits with only ferromagnetic and paramagnetic amorphous Sn-Fe phases present.

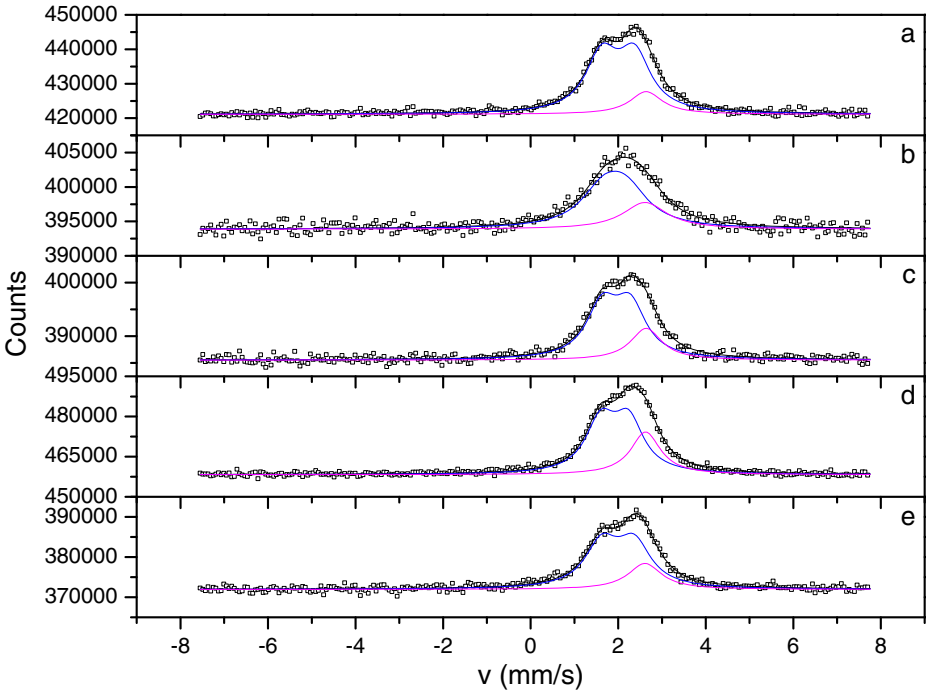

Fig. 3 ^{119}Sn Mössbauer spectra of pulse plated Sn-Ni deposits

The ^{119}Sn spectrum of the DC deposited Sn-Ni sample (Fig. 3a) was decomposed into a singlet and a broad doublet. The singlet is the fingerprint of β-Sn, while the doublet can be attributed to a paramagnetic amorphous or microcrystalline Sn-Ni phase. The Mössbauer spectra of all the pulse plated samples exhibited the same two spectral components. Due to the relatively low content (around 10 %) of nickel no ferromagnetic component appears in any of the spectra. XRD measurements complemented the Mössbauer results, only amorphous and small intensity β-Sn peaks appeared on the diffractograms. Pulse plating at the lowest peak current density (sample SnNi I) produces a deposit with a higher tin and lower nickel content, which is reflected on the corresponding Mössbauer spectrum (Fig. 3b) in an increased spectral amount of β-Sn and a decreased amount of the paramagnetic Sn-Ni phase. Applying a higher peak current density with the same on- and off-pulse time (sample SnNi III) results in a slight drop of tin content. Accordingly, in the Mössbauer spectrum of sample SnNi III (Fig. 3c) a decreased amount of β-Sn is observed, while the spectral amount of the paramagnetic Sn-Ni phase increases. Decreasing the relaxation time (sample SnNi VIII) produces an opposite effect on the deposit as the increase of the current density during the pulse. The tin content increases, reaching its maximum. It is reflected on the Mössbauer spectrum of sample SnNi VIII (Fig. 3d) in a further increased amount of β-Sn and a decreased spectral amount of the paramagnetic Sn-Ni phase. Increasing the on-pulse time (sample SnNi X) produces a deposit with the lowest tin and the highest nickel content. The Mössbauer spectrum of sample SnNi X (Fig. 3e) exhibits a drop in the spectral amount of β-Sn

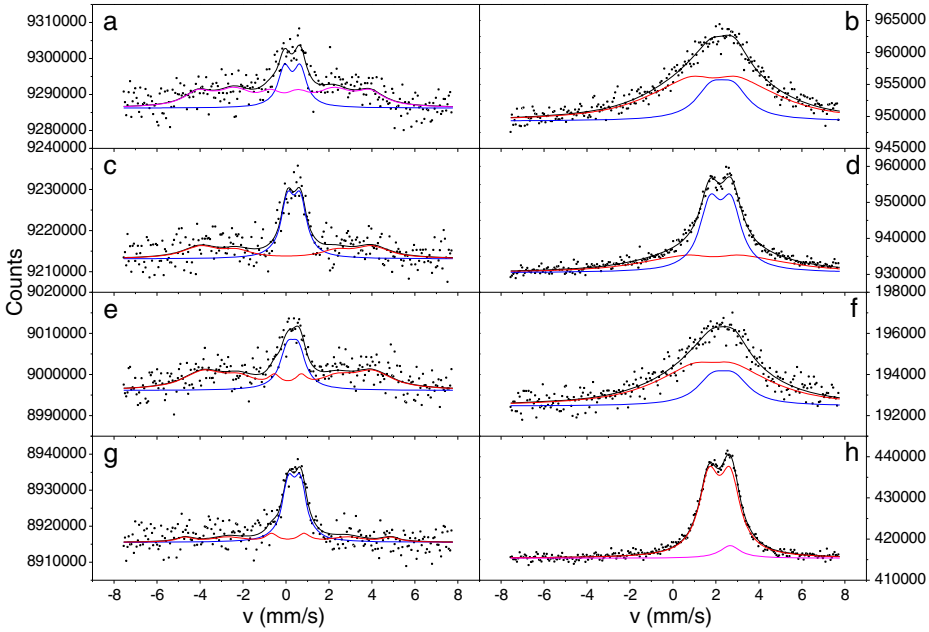

Fig. 4 ^{57}Fe (*left*) and ^{119}Sn (*right*) Mössbauer spectra of pulse plated Sn-Ni-Fe deposits

and an increase in the amount of the paramagnetic Sn-Ni phase, which changes were similar to those observed in the case of sample SnNi III deposited at an increased peak current density (Fig. 3c).

Pulse plating at the lowest peak current density in the Sn-Ni-Fe bath (sample SnNiFe I) produces a thin Sn-Ni-Fe deposit. The ^{57}Fe spectrum (Fig. 4a) of sample SnNiFe I was decomposed into a magnetically split sextet and a doublet with broad lines. The sextet was attributed to a ferromagnetic amorphous Sn-Ni-Fe phase, while the doublet was assigned to a paramagnetic amorphous Sn-Ni-Fe one. Similarly, the ^{119}Sn spectrum (Fig. 4b) was decomposed into a sextet and a doublet, which were associated with a ferromagnetic amorphous and a paramagnetic amorphous Sn-Ni-Fe phase, respectively. In both spectra, the ferromagnetic amorphous Sn-Ni-Fe phase is the dominant one. X-ray diffractograms of all the Sn-Ni-Fe samples exhibited broad amorphous peaks. Decreasing the relaxation time (sample SnNiFe IV) results in a small drop of tin content and an increase in nickel and iron content within the deposit. No new components appear in the ^{57}Fe and ^{119}Sn Mössbauer spectra (Fig. 4c and d) of sample SnNiFe IV, only the relative amount ratio of the ferromagnetic and paramagnetic Sn-Ni-Fe phases changes. The spectral amount of the paramagnetic component slightly increases on the expense of the ferromagnetic component's amount. Increasing the on-pulse time (sample SnNiFe X) induces a further increase in iron content and results in the lowest tin content. Nickel content decreases to the detection limit. An increase in the spectral amount of the ferromagnetic amorphous Sn-Ni-Fe phase is observed in the ^{57}Fe and ^{119}Sn Mössbauer spectra (Fig. 4e and f) of sample SnNiFe X, while the relative amount of the paramagnetic component decreases. The huge increase of the on-/off-pulse time and peak current density

(sample SnNiFe XIV) results in a deposit with the highest tin and nickel content and the lowest iron content. The ^{57}Fe spectrum (Fig. 4g) of sample SnNiFe XIV displays a significant decrease in the relative amount of the ferromagnetic amorphous Sn-Ni-Fe alloy, making the paramagnetic component the dominant one in this case. The ^{119}Sn spectrum (Fig. 4h) of sample SnNiFe XIV doesn't exhibit magnetic splitting. Besides the doublet, belonging to the paramagnetic amorphous Sn-Ni-Fe phase, a singlet, with a small relative amount (8 %), appears in the spectrum. The singlet is the fingerprint of β-Sn and appears due to a segregation, which only occurred during pulse plating using a long pulse and high peak current density.

4 Conclusion

Applying pulse electrodeposition technique we were able to produce new, amorphous binary and ternary alloy coatings. A fine tuning of the deposit composition and plating current efficiency can be established within these systems by meticulous variation of the deposition parameters.

We can conclude that the increase of the peak current density during pulse plating only has a small effect on the current efficiency and the composition of the Sn-Ni system. The Sn-Fe binary system shows larger sensitivity to the applied pulse current.

Summarizing the effect of the decrease of the relaxation time, the electrolyte around the cathode cannot be completely refreshed between the applied pulses. The concentration of metal ions depletes fast and mainly hydrogen evolution can remove the extra charge from the cathode surface, resulting in smaller current efficiency equally for the binary and ternary baths. In the case of the Sn-Ni binary system hydrogen evolution presumably inhibits the co-deposition of nickel; hence tin content could slightly increase.

For the Sn-Fe and Sn-Ni-Fe baths, the higher relaxation time results in the increase of tin content at the expense of iron content, obviously due to selective dissolution of iron from the alloy during the longer relaxation time.

The increase of the on-pulse time leads to a deposition regime, where the effect of switching the pulse on/off fades and the composition as well as the kinetics of the deposition could be controlled similarly to the case of the conventional direct current plating.

The structural changes occurring in the alloys deposited at different plating conditions were effectively monitored by the help of Mössbauer spectroscopy, and complemented by XRD measurements. It was shown that the pulse plated Sn-Fe and Sn-Ni-Fe deposits consist of ferromagnetic and paramagnetic amorphous alloy phases, without the presence of crystalline alloys exhibited in the DC deposited samples. The ferromagnetic amorphous alloy phase is the dominant one except for the cases of the Sn-Fe sample plated at the lowest peak current density, resulting in a deposit with the lowest iron content without a ferromagnetic phase, and the Sn-Ni-Fe sample plated at longer pulse times and highest peak current density, where the paramagnetic phase dominates and β-Sn segregation also occurs. Changes in the short-range order of the amorphous phases were observed, which correlated with the compositional changes within the samples. Increasing the content of iron and nickel gives rise to the relative amount of the ferromagnetic components with an increase in the value of the hyperfine magnetic field, while a decreased content of the

magnetic alloying elements results in deposits, where the amorphous paramagnetic alloy phases dominate.

Structurally, pulse plated Sn-Ni deposits are similar to DC deposited coatings. They consist of paramagnetic alloy phases and minor amounts of β-Sn, the relative amount of which correlates with the tin content of the samples. Due to the relatively low content of nickel no ferromagnetic component is present in the pulse plated Sn-Ni alloys.

Acknowledgement This work was supported by the Hungarian National Science Foundation (OTKA) under project no. T068135.

References

1. Kuzmann, E., Sziráki, L., Lak, G.B., Stichleutner, S., Havancsák, K., Süvegh, K., El-Sharif, M., Chisholm, C.U., Homonnay, Z., Vértes, A.: AIP Conf. Proc. **1489**, 3–12 (2012)
2. Lak, G.B., Kuzmann, E., El-Sharif, M., Chisholm, C.U., Stichleutner, S., Homonnay, Z., Sziráki, L.: Hyperfine Interact. **218**, 145–150 (2013)
3. Kuzmann, E., Stichleutner, S., Doyle, O., Chisholm, C.U., El-Sharif, M., Homonnay, Z., Vértes, A.: AIP Conf. Proc. **765**, 99–107 (2005)
4. El-Sharif, M., Chisholm, C.U., Kuzmann, E., Sziráki, L., Stichleutner, S., Homonnay, Z., Süvegh, K., Vértes, A.: Hyperfine Interact. **192**, 1–12 (2009)
5. Chisholm, C.U., El-Sharif, M., Kuzmann, E., Stichleutner, S., Homonnay, Z., Vértes, A.: Mater. Chem. Phys. **120**, 558–565 (2010)
6. Chisholm, C.U., Kuzmann, E., El-Sharif, M., Doyle, O., Stichleutner, S., Solymos, K., Homonnay, Z., Vértes, A.: Appl. Surf. Sci. **253**, 4348–4355 (2007)
7. Sziráki, L., Kuzmann, E., El-Sharif, M., Chisholm, C.U., Stichleutner, S., Lak, G.B., Süvegh, K., Tatár, E., Homonnay, Z., Vértes, A.: Appl. Surf. Sci. **256**, 7713–7716 (2010)
8. Sziráki, L., Kuzmann, E., Lak, G.B., El-Sharif, M., Chisholm, C.U., Stichleutner, S., Havancsák, K., Zih-Perényi, K., Homonnay, Z., Vértes, A.: Surf. Coat. Tech. **211**, 184–187 (2012)
9. Chandrasekar, M.S., Pushpavanam, M.: Electrochim. Acta **53**, 3313–3322 (2008)
10. Klencsár, Z., Kuzmann, E., Vértes, A.: J. Radioanal. Nuclear Chem. **210**, 105–118 (1996)